Novel Electroactive Polyamide 12 Based Nanocomposites Filled With Reduced Graphene Oxide

A. Dorigato, A. Pegoretti
Department of Industrial Engineering and INSTM Research Unit, University of Trento, Via Sommarive 9, Trento, 38123, Italy

Novel electroactive nanocomposites were prepared by adding to a polyamide 12 (PA12) matrix different amounts (from 1 to 8 wt%) of reduced graphene oxide (rGO), and the thermo-electrical behavior of the prepared bulk materials was compared with that of the corresponding fibers. FESEM micrographs on bulk materials highlighted an evident aggregation of the rGO lamellae, proportional to the filler concentration. The presence of rGO stacks was responsible of a heavy embrittlement of the samples, with a strong reduction of the elongation at break, and of the limited electrical conductivity of the samples (about 10^5 Ω·cm with a rGO amount of 4 wt%). Moreover, nanofiller addition determined an improvement of the thermal degradation resistance, associated to a slight drop of the glass transition temperature (about 7°C with a nanofiller concentration of 4 wt%) and of the crystallinity degree (up to 9% for an rGO loading of 4 wt%). The extrusion process adopted to prepare nanocomposite fibers caused a partial breakage of rGO aggregates and their progressive alignment along the drawing direction, determining thus an electrical resistivity increase with respect to the bulk samples. Therefore, the surface heating of the prepared fibers through Joule effect was possible only at elevated rGO amounts (i.e., 8 wt%). POLYM. ENG. SCI., 59:198–205, 2019. © 2018 Society of Plastics Engineers

INTRODUCTION

It is well known that nanofiller addition can noticeably improve the mechanical stability [1, 2] and the thermal degradation resistance [3–7] of polymer matrices. Furthermore, different techniques were recently adopted to develop conductive polymer composites [8, 9], thus overcoming the problems associated to the limited electrical conductivity of plastics [10, 11]. Electrically conductive polymers could find wide application in antistatic packaging films, in sensitive electronics and in electromagnetic shielding. As already reported in various papers of our group [12–18], one the most widely diffused techniques for the preparation of conductive composites is the dispersion of nanostructured conductive fillers within polymer matrices. In this sense, graphene seems to be one of the most interesting conductive nanofillers [19–21], because of its combination of outstanding mechanical [22, 23] and functional properties [24–28]. To overcome the problem of the dispersion of graphene layers within the polymer matrices [29], particular attention has been recently devoted to graphene oxide (GO) [30–33]. From a microstructural point of view, GO is constituted by planar sheets of carbon atoms with oxygen containing functionalities (e.g., hydroxyl, epoxide, and carbonyl groups), that are responsible of its hydrophilicity and its easy dispersability in water solutions [34, 35]. Therefore, polymer nanocomposites with intercalated/exfoliated morphology can be obtained [36, 37]. The subsequent reduction of GO through chemical agents (hydrazine derivatives) [38, 39] or thermal treatments [40, 41] can promote a recovery of the pristine graphitic structure of the material. Thermal reduction of GO [42, 43] seemed to be an easy and effective route to develop graphene based nanocomposites, but elevated temperatures (from 300°C to 1,000°C) are generally required to achieve a satisfactory GO reduction [44, 45]. This is the reason why this process generally requires polymers with elevated thermal stability [46, 47], like liquid-crystalline polymers (LCP) [48].

From an industrial point of view, polyamides (nylon 6, nylon 6,6, nylon 11, nylon 12, and nylon 6,10) has gained particular interest for the possibility of developing high value added fibers and bulk materials [49–51]. Thanks to its relative low melting temperature (about 180°C), PA12 represents an interesting replacement for several traditional plastics [52], and also innovative PA12 based blends and composites have been prepared in the last decades [53–55]. Among them, nanocomposites with organo-modified clays were probably the most widely investigated [56–59]. For instance, both polyamide 66 recycled fibers [60] and aramid regenerated fibers [61] were recently considered by our group as possible reinforcements for PA12 matrices. In another recent paper of our group, PA12 based nanocomposites filled with different carbonaceous nanofillers (CB, CNTs and xGnP) were successfully developed and characterized [62].

An interesting industrial perspective is represented by the possibility to utilize non-woven polyamide 12 fabrics produced through spunbond or meltblown technology as air/liquid filters in automotive applications [63]. A similar operation has been already conducted by our group in the preparation of melt-blown filters based on organo-modified clay (OMC)-PA6 nanocomposites [63]. On the basis of these considerations, in this work innovative PA12 based nanocomposites filled with different amounts of reduced graphene oxide were investigated. Considering our partnership with a producer of non vowen fluid filters for the automotive field (i.e., UFI Innovation Center Srl), this investigation can be considered as a part of a wider project focused on the development of electroactive melt blown filters. The role played by nanofiller addition on the physical performances of the bulk materials was investigated, and a comparison with the properties of the corresponding fibers was then performed.

EXPERIMENTAL PART

Materials

Polymer granules of Rilsan PA12, provided by Arkema (Philadelphia) were used (melting point 178°C, density 1.02 g/cm^3). Graphite powder (particle size < 20 μm) was provided by

Correspondence to: A. Dorigato; e-mail: andrea.dorigato@unitn.it
Contract grant sponsor: Fondazione Cassa di Risparmio di Trento e Rovereto (CARITRO) ("Bando Caritro 2014 per progetti di ricerca scientifica finalizzati allo sviluppo di iniziative imprenditoriali."); contract grant sponsor: National Interuniversitary Consortium of Materials Science and Technology (INSTM).
DOI 10.1002/pen.24889
Published online in Wiley Online Library (wileyonlinelibrary.com).

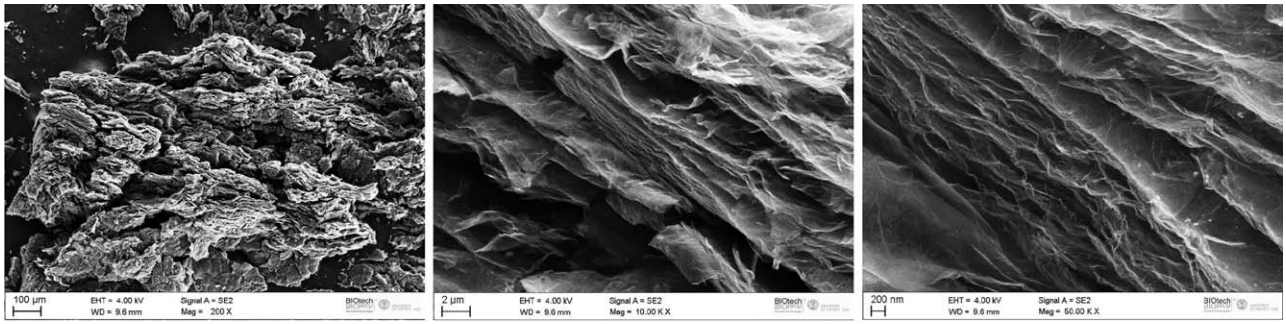

FIG. 1. FESEM images of the rGO powder at different magnifications.

Sigma-Aldrich. All other reagents with analytical grade purity were used as received.

Samples Preparation

Preparation of rGO Nanofiller. Graphite oxide was prepared from graphite powder through a modified Hummers method [64, 65]. Graphite powder was oxidized through sulfuric acid and potassium permanganate, dispersed in water and exfoliated through a sonicator, to obtain graphene oxide (GO). The detailed procedure to obtain GO solutions was described in our previous work on graphene nanocomposites [41]. The resulting GO solution was then dried at 40°C under vacuum for 24 h to obtain thin films of GO. Preliminary DSC tests on dried GO films under a nitrogen atmosphere (not reported for the sake of brevity) showed the existence of an exothermic peak located at 204°C, associated to the thermal reduction of the GO. Therefore, GO films were thermally treated in a furnace at 350°C for 15 min, to obtain powder of reduced graphene oxide (rGO). The obtained GO and rGO fillers showed electrical resistivity values of 6.94×10^2 Ω·cm and 3.30×10^{-1} Ω·cm, respectively, confirming thus that the thermal reduction of GO effectively occurred. Figure 1 reports FESEM images of the obtained rGO powder at different maginifcation levels. It can be noticed the presence of single thin graphene lamellae stacked in aggregated structures.

Preparation of Nanocomposite Materials. PA12 granules were preliminary dried at 80°C for 6 h with an air flow of 7 Nm^3/h in a Moretto X Dry Air drier. Polymer chips and the rGO nanofiller were then melt-compounded for 5 min in a Thermo-Haake Polylab Rheomix 600p operating at 200°C and 50 rpm. The compounded samples were then hot-pressed at 200°C for 5 min applying a pressure of 0.33 MPa, to obtain square sheets with thickness values between 1.0 and 1.2 mm. In this way, nanocomposite samples with rGO amounts from 1 to 4 wt% were produced. The prepared samples were then stored in a vacuum bag to avoid moisture absorption.

A part of the prepared bulk materials was then grinded to feed an Estru 13 single screw extruder (Friul Filiere, Udine, Italy), having a L/d ratio of 15 and a screw diameter of 14 mm. A screw speed of 30 rpm and a temperature profile of 180/200/200/200°C were adopted. Polymer fibers of neat PA12 and of 4 wt% rGO filled nanocomposite were thus produced. Moreover, a nanocomposite fiber at elevated rGO amount (i.e., 8 wt%) was also prepared, to maximize the electrical conductivity properties of nanofilled samples. The prepared filaments were then drawn at 100°C applying different draw ratios. In Table 1, the list of the prepared samples is reported.

Experimental Methodologies

The cryofractured surfaces of bulk materials and of the fibers were observed through a Zeiss Supra 40 field emission scanning electron microscope (FESEM). DSC measurements were performed both on bulk specimens and on the fibers with a Mettler DSC30 calorimeter under a nitrogen flow of 100 mL/min. A first heating from 0°C to 240°C was followed by a cooling stage from 240°C to 0°C and by a second heating from 0°C to 240°C, and all the thermal ramps were conducted at 10°C/min. The temperatures associated to the glass transition (T_g), the melting (T_m), and crystallization (T_c) of the polymer matrix were thus determined. The crystallinity degree (X_c) was computed as the ratio between the melting enthalpy of the samples and the reference value of the fully crystalline PA12 (i.e., 95 J/g [66]), taking into account also the effective weight concentration of PA12 in the samples. Thermogravimetric analysis (TGA) was performed through a Mettler TG50 thermobalance under an air flow of 150 mL/min in a temperature interval between 30°C and 700°C, at a heating rate of 10°C/min. The temperature associated to a mass loss of 5% ($T_{5\%}$) and the decomposition temperature (T_d), that is, the temperature related to the maximum mass loss rate, were computed.

The tensile properties under quasi-static conditions of bulk samples were measured at 23°C through an Instron 4502 tensile machine, testing ISO 527 type 1BA specimens (gage length 30 mm, width 5 mm, thickness 1.2 mm, distance between the grips 55 mm). Tests for the determination of the elastic modulus (E) were carried out at 0.25 mm/min, setting a maximum deformation of 1%. The strain was monitored using an Instron model

TABLE 1. List of the prepared samples.

Sample code	rGO weight concentration (wt%)	rGO volume concentration (vol%)	Sample type
PA12	—	—	bulk and fiber
PA12-rGO-1	1	0.46	bulk
PA12-rGO-2	2	0.93	bulk
PA12-rGO-3	3	1.40	bulk
PA12-rGO-4	4	1.88	bulk and fiber
PA12-rGO-8	8	3.75	bulk and fiber

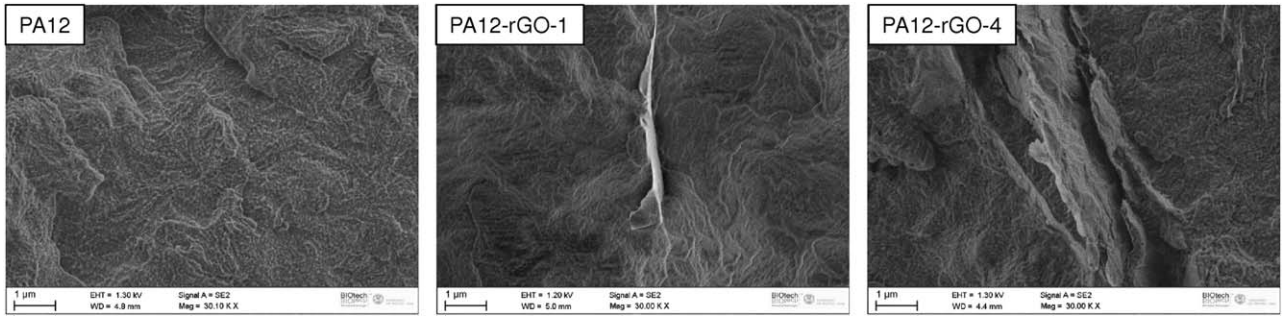

FIG. 2. FESEM images of the fracture surface of neat PA12 and of the relative nanocomposites (bulk materials).

2620–601 resistance extensometer with a gauge length 12.5 mm. The elastic modulus was measured as a secant value between strain levels of 0.05% and 0.25%. Tensile tests at break were performed without any extensometer at a crosshead speed of 10 mm/min to measure the ultimate tensile strength (UTS) and the strain at UTS (ε_{UTS}). Tensile tests on neat PA12 and nanocomposite fibers prepared at different draw ratio were carried out through an Instron 4502 tensile machine with a load cell of 10 N. Elastic modulus of fibers having a gage length of 30 mm was measured at a crosshead speed of 1 mm/min, while tensile properties at break (σ_b, ε_b) were determined at 50 mm/min. For all the tensile tests, five specimens were tested for each sample.

Electrical volume resistivity of bulk samples was evaluated in direct current mode at room temperature using a Keithley 6517A electrometer. ASTM D257 square film specimens, having a length of 95 mm and a thickness of 1 mm, were tested using coaxial electrodes. The bulk electrical resistivity (ρ) was computed through the expression reported in *Eq. 1*:

$$\rho = R \cdot \frac{\pi a^2}{t} \tag{1}$$

where R is the electrical resistance, a is the ray of the testing electrode, t is the thickness of the samples. Electrical resistivity of the fibers was determined at a distance between the testing electrodes of 30 mm. The surface temperature evolution on voltage applications was determined on fiber specimens through a Fluke TiRx thermographic camera, applying the electrodes on the fibers at a distance of 30 mm. The surface temperature was measured starting from 25°C, applying voltages of 200 and 220 V.

RESULTS AND DISCUSSION

Characterization of Bulk Materials

The morphological features of the prepared samples were investigated by FESEM observations (see Fig. 2). As expected, the surface of the neat PA12 sample appears to be quite corrugated, because of some plasticization phenomena that occurred during the tensile test. Observing the PA12-rGO-1 sample, it is possible to notice the presence of rGO aggregates homogeneously distributed within the matrix, with a mean length of 6 μm and a thickness of 500 nm. Increasing the filler amount up to 4 wt%, the dimension of these aggregates increases, and stacks of rGO lamellae 18 μm long and 1 μm thick can be observed. It can be hypothesized that the shear stresses generated during the melt compounding process were not able to completely break and disperse the nanofiller aggregates within the matrix. Moreover, the observed aggregation could be responsible of a significant deterioration of the physical properties of the prepared composite and to impede the formation of an electrical percolating network within the samples.

It could be also important to investigate the influence of the rGO lamellae on the thermal behavior of the bulk materials. Therefore, DSC tests were carried out on bulk materials. DSC thermograms of nanocomposites with different rGO contents collected during the first heating and the cooling scans are respectively shown in Fig. 3a and in b, while the most important results are summarized in Table 2. In general, a slight decrease

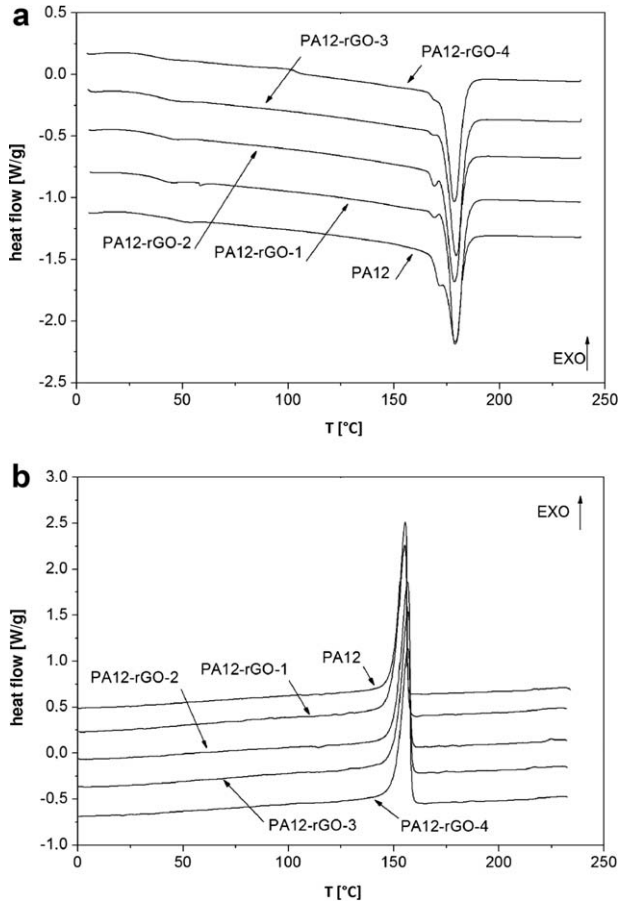

FIG. 3. DSC thermograms of neat PA12 and of the relative nanocomposites (bulk materials). (a) First heating stage, (b) cooling stage.

 DOI 10.1002/pen

TABLE 2. Results of DSC and TGA tests on neat PA12 and relative nanocomposites (bulk samples).

Sample	T_g (°C)	T_m (°C)	X_1 (%)	T_c (°C)	$T_{5\%}$ (°C)	T_d (°C)
PA12	47.3	179.1	68.9	155.6	378.0	478.3
PA12-rGO-1	39.6	179.0	56.2	155.3	406.3	471.3
PA12-rGO-2	42.8	178.6	63.9	156.6	394.3	472.0
PA12-rGO-3	37.9	179.3	63.2	156.8	408.0	477.3
PA12-rGO-4	39.7	178.8	60.0	156.7	404.0	479.7

T_g, glass transition temperature (first heating run); T_m, melting temperature (first heating run); X_1, crystallinity degree (first heating run); T_c, crystallization temperature (cooling run); $T_{5\%}$, temperature corresponding to a mass loss of 5%; T_d, decomposition temperature.

of the glass transition temperature (T_g) with respect to the neat PA12 can be detected for all the samples. Interestingly, an opposite trend was shown in our previous paper on the thermoelectrical properties of PA12 based nanocomposites filled with carbon black and carbon nanofibers [62]. It could be hypothesized that the lamellar structure of rGO aggregates can promote the mobility of polymer macromolecules above room temperature, thus decreasing the T_g values. The T_g decrease on rGO addition was also confirmed by dynamical mechanical analysis (not reported for the sake of brevity). It is evident that both the melting and the crystallization temperatures (T_m, T_c) of the materials are not significantly affected by the presence of nanofillers, while the crystallinity degree is slightly impaired by rGO addition. Contrarily to what observed in our paper on PA12 based nanocomposites [62] and on PBT/organoclay nanocomposites [63], in the present case nanofiller addition does not play nucleating role for the crystallization processes.

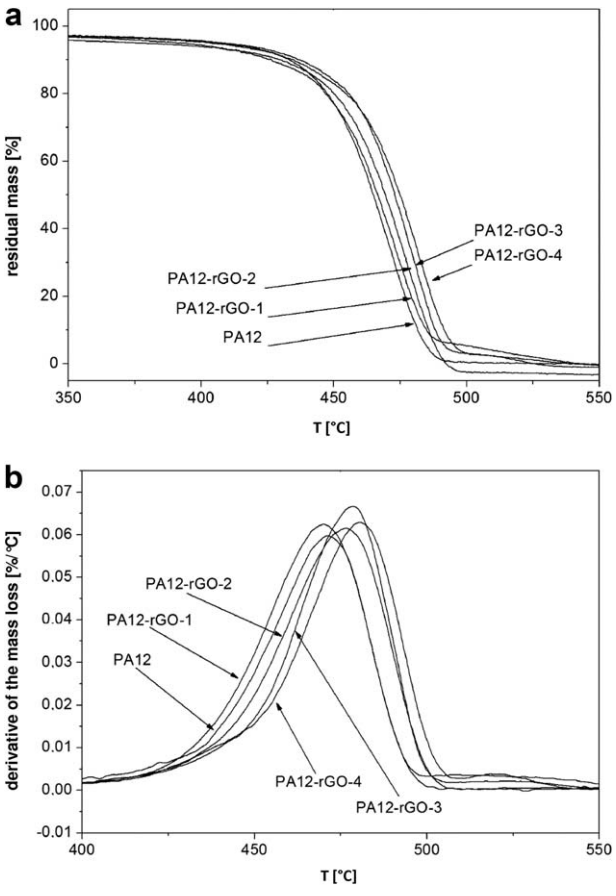

FIG. 4. Thermogravimetric curves of neat PA12 and of the relative nanocomposites (bulk materials). (a) Residual mass, (b) derivative of the mass loss.

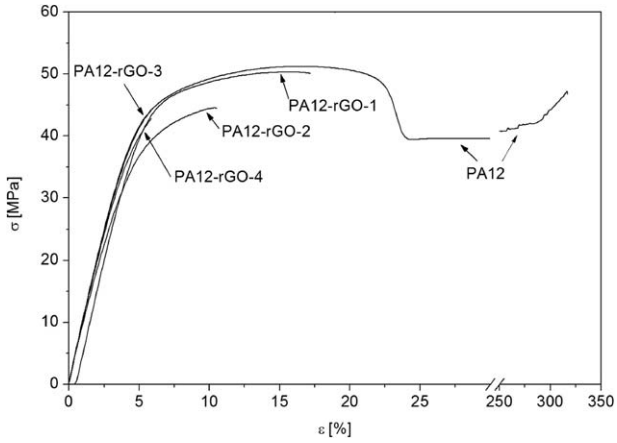

FIG. 5. Representative stress-strain curves of neat PA12 and of the relative nanocomposites (bulk materials).

The investigation of the thermal degradation behavior of the prepared materials could be important to hypothesize a future application as electroactive filters. This is the reason why thermogravimetric tests were performed on bulk specimens. In Fig. 4a, residual mass curves of neat PA12 and relative nanocomposites are reported, while in Fig 4b the derivative values of the mass loss are represented. It is important to underline that all the prepared samples are characterized by a single degradation step at about 470°C, and that the presence of reduced graphene oxide is responsible of a substantial increase of the $T_{5\%}$ values (up to 26°C with a rGO amount of 4 wt%). As reported in Table 2, the degradation temperature (T_d) seems to be not substantially affected by nanofiller addition. The observed increment in the thermal degradation resistance of the nanocomposite samples has been already reported in literature [67]. It is generally thought that graphene nanoplatelets create a tortuous path for air, delaying thus the thermo-oxidative degradation of the material [68].

In Fig. 5, representative stress-strain curves obtained from the tensile tests on neat PA12 and relative nanocomposites are shown, while the most important mechanical parameters are summarized in Table 3. A slight increment of the elastic modulus, proportional to the filler concentration, can be detected. As an example, at a rGO concentration of 4 wt% it is possible to increase the elastic modulus of about 8% with respect to neat PA12. Conversely, the rGO aggregation observed in FESEM micrographs (see Fig. 2) is probably responsible of the heavy

TABLE 3. Results of quasi-static tensile tests on neat PA12 and relative nanocomposites (bulk samples).

Sample	E (MPa)	UTS (MPa)	ε_{UTS} (%)
PA12	1412 ± 39	51.8 ± 0.4	254.3 ± 57.3
PA12-rGO-1	1397 ± 44	50.1 ± 0.2	15.7 ± 0.2
PA12-rGO-2	1432 ± 26	44.0 ± 1.5	10.6 ± 2.1
PA12-rGO-3	1477 ± 54	43.7 ± 5.0	7.1 ± 2.9
PA12-rGO-4	1529 ± 35	42.6 ± 6.2	6.8 ± 2.3

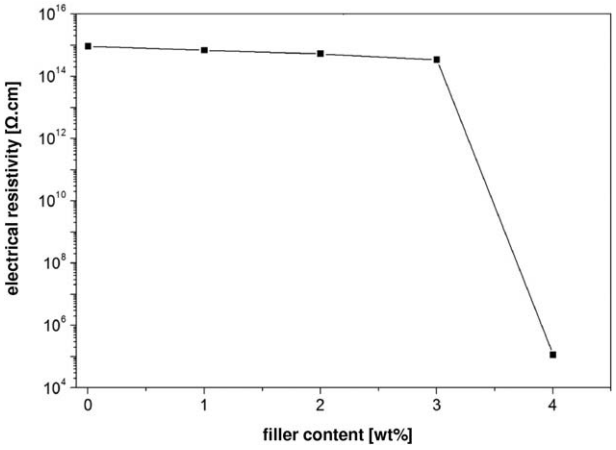

FIG. 6. Electrical resistivity values of neat PA12 and of the relative nanocomposites (bulk materials).

embrittlement measured of the samples, with a reduction of the ε_{UTS} even at limited rGO contents. It could be also important to underline that the ultimate tensile values are not dramatically impaired by nanofiller introduction.

Bulk electrical resistivity values as a function of the rGO content are reported in Fig. 6. It is immediately evident that the addition of a proper amount (higher than 3 wt%) of reduced graphene oxide in the PA12 matrix can promote a reduction of electrical resistivity down to 10^5 Ω·cm at a filler concentration of 4 %wt. In our previous work on PA12 nanocomposites [62] an electrical resistivity value of 1.8×10^3 Ω·cm was obtained by adding a mixture of carbon black and carbon nanofibers at a total filler loading of 4 wt%. The industrial partner (UFI Innovation Center Srl) involved in this research indicated a resistivity value equal or lower than 10^3 Ω·cm as the technical requirement to obtain non woven filters that could be effectively heated through Joule effect [69]. Therefore, further efforts will be made in the future to improve nanofiller dispersion and to achieve higher electrical conductivity values. Conversely, at rGO concentration above 4 wt% the viscosity of the matrix in the molten state is be too high, and the processability of these materials through melt blowing technology would be seriously impaired. To investigate the theoretical possibility to obtain conductive materials that could be effectively heated through Joule effect, also a nanocomposite sample at elevated filler amount (i.e., 8 wt%) was prepared through melt compounding (for higher filler contents the viscosity of the matrix would be too high also for a common extrusion process), and the physical properties of neat PA12, PA12-rGO-4, and PA12-rGO-8 fibers were then evaluated.

TABLE 4. Results of DSC tests on neat PA12 and relative nanocomposites fibers at different draw ratios.

Sample	T_g (°C)	T_m (°C)	X_1 (%)	T_c (°C)
PA12-dr1	46.6	178.4	61.2	153.5
PA12-dr2	49.3	177.9	61.2	153.7
PA12-dr3	53.4	178.1	62.7	153.5
PA12-rGO-4-dr1	49.5	177.9	47.0	157.4
PA12-rGO-4-dr2	52.9	178.6	53.8	157.6
PA12-rGO-4-dr3	53.8	178.6	52.3	157.6
PA12-rGO-8-dr1	45.0	177.1	42.0	157.9
PA12-rGO-8-dr2	47.1	178.4	44.7	158.1
PA12-rGO-8-dr3	48.4	177.9	44.0	158.0

T_g, glass transition temperature (first heating run); T_m, melting temperature (first heating run); X_1, crystallinity degree (first heating run); T_c, crystallization temperature (cooling run).

Characterization of the Fibers

Neat PA12 and nanocomposite fibers were prepared and drawn at different draw ratios, and the microstructural behavior of the prepared fibers was then investigated. In Fig. 7, representative FESEM images of the fracture surface of nanocomposite fibers are reported. From a qualitative point of view, the observed morphology is not so different from that of the corresponding bulk materials, and rGO aggregates homogeneously dispersed within the matrix are still present. However, the extrusion process promotes a partial exfoliation/orientation of rGO aggregates with a consequent reduction of their size. For instance, the microstructure of the undrawn PA12-rGO-4 fiber (i.e., at DR = 1) is characterized by the presence of rGO stacked lamellae having a length of 4 μm and a thickness of 200 nm. The same microstructural behavior is observed for the undrawn PA12-rGO-8 fiber. The drawing process induces a reduction of the dimension of the rGO aggregates. In fact, in PA12-rGO-8 fiber with DR = 3 the length of the rGO aggregates (i.e., 2 μm) is reduced with respect to the corresponding fibers. As reported in our previous paper on polyethylene nanocomposite fibers [70], the drawing process produces the rupture of nanofiller aggregates and their alignment along the strain direction. A similar process was also able to induce an evident exfoliation in polymer/clay nanocomposites [71].

The thermal behavior of the prepared fibers was also evaluated. In Table 4, the results of DSC tests on neat PA12 and on the relative nanocomposite fibers as a function of the draw ratio

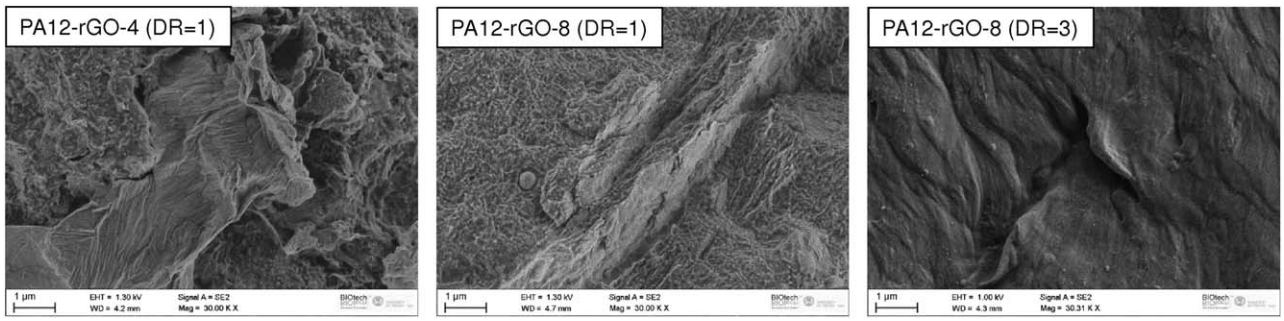

FIG. 7. FESEM images of the cryofractured cross section of PA12 based nanocomposites fibers.

 DOI 10.1002/pen

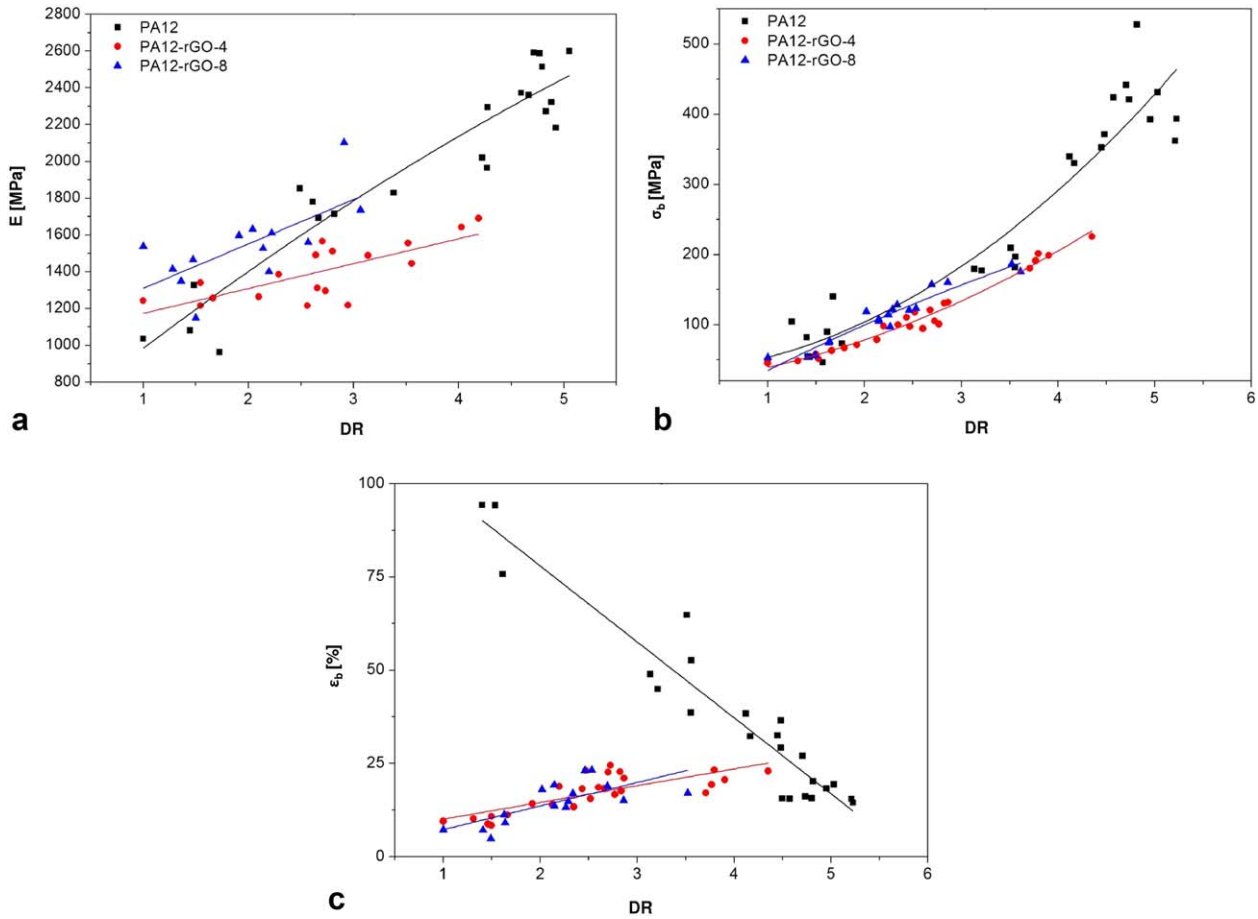

FIG. 8. Quasistatic tensile properties of PA12 and relative nanocomposites fibers as a function of the draw ratio. (a) Elastic modulus, (b) stress at break, (c) strain at break. [Color figure can be viewed at wileyonlinelibrary.com]

are reported. A DR increase determines an increase both of the T_g and of the crystallinity degree (X_c) of the material. It is probable that the alignment of macromolecules induced by the drawing process promotes the crystallization and the immobilization of the amorphous fractions within the matrix. Interestingly, the crystallinity values of the nanofilled fibers are systematically lower than those of the unfilled ones at the same draw ratio. It can be, therefore, concluded that the presence or rGO hindered the crystallization process of the materials.

The tensile properties of the prepared fibers were also determined, and in Fig. 8a the elastic modulus values at different draw ratios are reported, while in Fig. 8b and c the stress at break (σ_b) and strain at break values (ε_b) are respectively shown. As expected, as the draw ratio increases a systematic enhancement of the material stiffness is induced, regardless the filler amount. Considering the elastic modulus at DR = 1, the nanofiller introduction leads to a stiffness increase, proportionally to the rGO loading. At DR = 3, an opposite situation can be seen, and the stiffness of unfilled fibers is even higher than that of the nanocomposite ones (see Fig. 8a). To explain this result, a partial fiber-matrix debonding at elevated draw ratio can be hypothesized. However, further investigations are required to explain this behavior. For as the stress at break is concerned (Fig. 8b), it can be concluded that nanofiller introduction does not substantially affect the strength of the fibers. Reduced graphene oxide determines a substantial embrittlement of the samples, and ε_b values of the nanocomposite fibers are systematically lower than those detected for the neat PA12 fibers (Fig. 8c). As it often happens in polymer fibers [72], a DR increase determines a decrease of the strain at break values, while ε_b values of the nanofilled fibers are very limited even at DR = 1 and thus practically unaffected by the drawing operation.

In view of the future application of these materials as electroactive melt blown filters, electrical conductivity tests were carried out on the fibers. In Table 5, electrical conductivity values of neat PA12 and nanocomposite fibers at two different DR are reported. It is interesting to note how for the PA12-rGO-4 fiber the extrusion process is responsible of a significant electrical resistivity enhancement with respect to the corresponding

TABLE 5. Electrical resistivity of neat PA12 and relative nanocomposite fibers at DR = 1 and DR = 3.

Sample	Resistivity (Ω·cm)
PA12-dr1	1.7 E +12
PA12-rGO-4-dr1	1.3 E +12
PA12-rGO-8-dr1	9.8 E +11
PA12-dr3	1.7 E +12
PA12-rGO-4-dr3	8.3 E +11
PA12-rGO-8-dr3	1.1 E +04

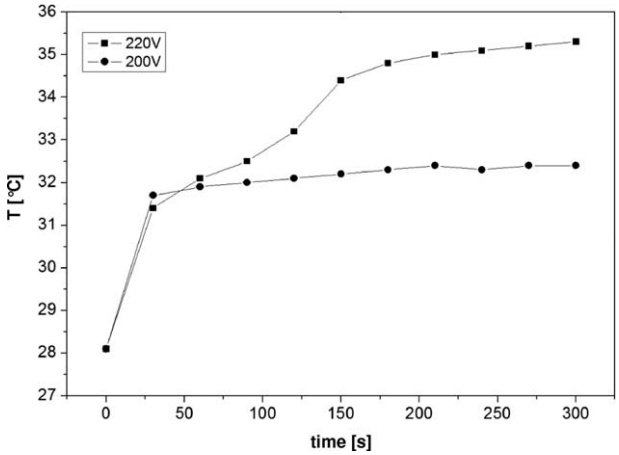

FIG. 9. Surface temperature evolution of the PA12-rGO-8 fiber with DR = 3 with an applied voltage of 200 V and 220 V.

bulk material, and the electrical percolation threshold cannot be reached even for a rGO amount of 8 wt%. A possible explanation of this result can be found in our previous paper on PA12 based nanocomposites [27]. In that work, it was shown how the orientation of the nanofiller along the drawing direction limited the possibility of lateral connection between the rGO lamellae, delaying the formation of a conducting path within the material and decreasing the electrical resistivity of the material. On the contrary, in bulk samples the random orientation of the filler promotes the formation of the conductive path at lower concentrations with respect to the corresponding fibers. Therefore, increasing the draw ratio at 3, a relatively low resistivity value (1.1×10^4 Ω·cm) can be obtained only with a rGO content of 8 wt%. At elevated draw ratio, the lateral connections between aligned rGO aggregates are formed, and the restoration of a conductive path within the material is, therefore, possible. On the basis of the above considerations, it is, therefore, clear why an effective heating of the nanocomposite fibers through Joule effect could be observed only with a rGO content of 8 wt% and with DR = 3. From Fig. 9, it is evident that only PA12-rGO-8 fibers are characterized by interesting surface temperature increase once a voltage is applied. A temperature of 32°C was reached after 300 s with a tension of 200 V, while with 220 V a higher temperature (i.e., 35°C) can be achieved in the same time interval. Another interesting aspect is that during the first seconds a rapid temperature increase occurs, and the material reaches a constant temperature after 150 s, because the generated thermal power is equal to the dissipated one. This aspect is very important for the final application of these materials as electroactive filters, because the thermal degradation of the materials for prolonged voltage application times should be avoided. It is, therefore, confirmed the theoretical potential of the prepared fibers in the development of electroactive filters, but further efforts will be required to lower their electrical percolation threshold and increase the electrical conductivity.

CONCLUSIONS

In this work a PA12 matrix was melt compounded with thermally reduced graphene oxide (rGO), and the thermo-electrical properties of the resulting materials in bulk and fiber form were investigated. FESEM micrographs evidenced how rGO aggregation tendency increased with the nanofiller amount, and this microstructural feature limited the possibility to obtain nanocomposites with resistivity values lower than 10^5 Ω·cm (at an rGO concentration of 4%wt). Moreover, the presence of rGO stacked lamellae determined a progressive embrittlement of the samples. Conversely, nanofiller addition determined a slight increase of the glass transition temperature, of the crystallinity degree, of the thermal resistance and of the stiffness of bulk materials. The breakage of nanofiller aggregates and their alignment along the drawing direction evidenced in FESEM images was responsible of an electrical resistivity enhancement with respect to the corresponding bulk samples. For these materials, a higher rGO content is required to observe an effective surface heating through Joule effect.

ACKNOWLEDGMENTS

Mr. Fabrizio Sottini is gratefully acknowledged for his support to the experimental work.

REFERENCES

1. T. Agag, T. Koga, and T. Takeichi, *Polymer*, **42**, 3399 (2001).
2. Y.M. Cao and Q.K. Wu, *J Shanghai Jiaotong Univ, (Medical Science)*, **37**, 110 (2017).
3. X. Fu and S. Qutubuddin, *Mater. Lett.*, **42**, 12 (2000).
4. D.G. Papageorgiou, I.A. Kinloch, and R.J. Young, *Prog. Mater. Sci.*, **90**, 75 (2017).
5. J.S. Shelley, P.T. Mather, and K.L. De Vries, *Polymer*, **42**, 5849 (2001).
6. Z. Shu, G. Chen, and Z. Qi, *Plast. Ind.*, **28**, 24 (2000).
7. F.M. Uhl and C.A. Wilkie, *Polym. Degrad. Stab.*, **76**, 111 (2002).
8. M. Armand, *Adv. Mater.*, **2**, 278 (1990).
9. T.A. Ibidapo, *Polym. Eng. Sci.*, **28**, 1473 (1988).
10. A. Kausar and S. Anwar, *Polym. –Plast. Technol. Eng.*, **57**, 565 (2018).
11. R.H. Norman and B.B. Boonstra, *J. Polym. Sci. Part B: Polym. Phys.*, **10**, 479 (1972).
12. A. Biani, A. Dorigato, W. Bonani, M. Slouf, and A. Pegoretti, *Express Polym. Lett.*, **10**, 977 (2016).
13. A. Dorigato, V. de Freitas, J.A. Covas, M.C. Paiva, M. Brugnara, and A. Pegoretti, *J. Elastomers Plast.* (in press).
14. A. Dorigato, G. Giusti, F. Bondioli, and A. Pegoretti, *Express Polym. Lett.*, **7**, 673 (2013).
15. A. Dorigato and A. Pegoretti, *Polym. Eng. Sci.*, **57**, 537 (2017).
16. A. Dorigato and A. Pegoretti, *Polym. Eng. Sci.*, **58**, 430 (2018).
17. D. Pedrazzoli, A. Dorigato, and A. Pegoretti, *J. Nanosci. Nanotechnol.*, **12**, 4093 (2012).
18. D. Pedrazzoli, A. Dorigato, and A. Pegoretti, *Compos. Part A Appl. Sci. Manuf.*, **43**, 1285 (2012).
19. A.M. Díez-Pascual, J.A.L. Sánchez, R.P. Capilla, and P.G. Díaz, *Polymers*, **10**, 217 (2018).
20. A.K. Geim and K.S. Novoselov, *Nat. Mater.*, **6**, 183 (2007).
21. T. Kuila, S. Bose, A.K. Mishra, P. Khanra, N.H. Kim, and J.H. Lee, *Prog. Mater. Sci.*, **57**, 1061 (2012).
22. H. Kim, A.A. Abdala, and C.W. Macosko, *Macromolecules*, **43**, 6515 (2010).

23. M.A. Rafiee, J. Rafiee, I. Srivastava, Z. Wang, H. Song, Z.Z. Yu, and N. Koratkar, *Small*, **6**, 179 (2010).
24. S. Ganguli, A.K. Roy, and D.P. Anderson, *Carbon*, **46**, 806 (2008).
25. M.T. Hung, O. Choi, Y.S. Ju, and H.T. Hahn, *Appl. Phys. Lett*., **89**, 023117 (2006).
26. K. Kalaitzidou, H. Fukushima, and L.T. Drzal, *Carbon*, **45**, 1446 (2007).
27. M. Tait, A. Pegoretti, A. Dorigato, and K. Kalaitzidou, *Carbon*, **49**, 4280 (2011).
28. H. Wu and L.T. Drzal, *Polym. Compos*., **34**, 2148 (2013).
29. N. Saravanan, R. Rajasekar, S. Mahalakshmi, T.P. Sathishkumar, K.S.K. Sasikumar, and S. Sahoo, *J. Reinforced Plast. Compos*., **33**, 1158 (2014).
30. X. Du, Z.Z. Yu, A. Dasari, J. Ma, M. Mo, Y. Meng, and Y.W. Mai, *Chem. Mater*., **20**, 2066 (2008).
31. A. Nag, A. Mitra, and S.C. Mukhopadhyay, *Sens. Actuators, A: Phys*., **270**, 177 (2018).
32. S. Stankovich, R.D. Piner, S.T. Nguyen, and R.S. Ruoff, *Carbon*, **44**, 3342 (2006).
33. G. Wang, B. Wang, J. Park, J. Yang, X. Shen, and J. Yao, *Carbon*, **47**, 68 (2009).
34. S. Park, J. An, I. Jung, R.D. Piner, S.J. An, X. Li, A. Velamakanni, and R.S. Ruoff, *Nano Lett*., **9**, 1593 (2009).
35. S. Stankovich, R.D. Piner, X. Chen, N. Wu, S.T. Nguyen, and R.S. Ruoff, *J. Mater. Chem*., **16**, 155 (2006).
36. F.T. Cerezo, C.M.L. Preston, and R.A. Shanks, *Macromol. Mater. Eng*., **292**, 155 (2007).
37. Z.R. Ying, Z.M. Dang, X.H. Yan, X. Ouyang, and Y.Y. Gao, *Adv. Mater. Res*., **335–336**, 347 (2011).
38. S. Gilje, S. Han, M. Wang, K.L. Wang, and R.B. Kaner, *Nano Lett*., **7**, 3394 (2007).
39. S. Park, J. An, J.R. Potts, A. Velamakanni, S. Murali, and R.S. Ruoff, *Carbon*, **49**, 3019 (2011).
40. W. Chen, L. Yan, and P.R. Bangal, *Carbon*, **48**, 1146 (2010).
41. M. Traina and A. Pegoretti, *J. Nanoparticle Res*., **14**, 1 (2012).
42. B. Dai, L. Fu, L. Liao, N. Liu, K. Yan, Y. Chen, and Z. Liu, *Nano Res*., **4**, 434 (2011).
43. K. Yin, H. Li, Y. Xia, H. Bi, J. Sun, Z. Liu, and L. Sun, *Nano-Micro Lett*., **3**, 51 (2011).
44. R. Sengupta, M. Bhattacharya, S. Bandyopadhyay, and A.K. Bhowmick, *Prog. Polym. Sci*., **36**, 638 (2011).
45. Y. Zhu, S. Murali, W. Cai, X. Li, J.W. Suk, J.R. Potts, and R.S. Ruoff, *Adv. Mater*., **22**, 3906 (2010).
46. K. Liu, L. Chen, Y. Chen, J. Wu, W. Zhang, F. Chen, and Q. Fu, *J. Mater. Chem*., **21**, 8612 (2011).
47. Y. Zhu, M.D. Stoller, W. Cai, A. Velamakanni, R.D. Piner, D. Chen, and R.S. Ruoff, *ACS Nano*, **4**, 1227 (2010).
48. D. Pedrazzoli, A. Dorigato, T. Conti, L. Vanzetti, M. Bersani, and A. Pegoretti, *Express Polym. Lett*., **9**, 709 (2015).
49. B. Benobeidallah, A. Benhamida, A. Dorigato, A. Sola, M. Messori, and A. Pegoretti, *J. Renew. Mater*., (in press).
50. M. Chanda and S.K. Roy, *Plastics Technology Handbook*, 4th ed., CRC Press, Boca Raton, FL (2007).
51. M.I. Kohan, *Nylon Plastics Handbook*, Carl Hanser Verlag, Munich, Germany (1995).
52. D. Bashford, *Thermoplastics: Directory and Databook*, Springer, Netherlands (1997).
53. S. Jose, S.V. Nair, S. Thomas, and J. Karger-Kocsis, *J. Appl. Polym. Sci*., **99**, 2640 (2006).
54. M. Sarkissova, C. Harrats, G. Groeninckx, and S. Thomas, *Compos. Part A: Appl. Sci. Manuf*., **35**, 489 (2004).
55. T. Tang, Z. Lei, and B. Huang, *Polymer*, **37**, 3219 (1996).
56. B. Alexandre, D. Langevin, P. Mederic, T. Aubry, H. Couderc, Q.T. Nguyen, A. Saiter, and S. Marais, *J. Membr. Sci*., **328**, 186 (2009).
57. B. Alexandre, S. Marais, D. Langevin, P. Médéric, and T. Aubry, *Desalination*, **199**, 164 (2006).
58. A. Hasook, H. Muramatsu, S. Tanoue, Y. Iemoto, and T. Unryu, *Polym. Compos*., **29**, 1 (2008).
59. Y. Zhang, J.H. Yang, T.S. Ellis, and J. Shi, *J. Appl. Polym. Sci*., **100**, 4782 (2006).
60. A. Dorigato and L. Fambri, *Polym. Compos*., **32**, 786 (2011).
61. A. Dorigato and L. Fambri, *J. Reinforced Plast. Compos*., **32**, 1243 (2013).
62. A. Dorigato, M. Brugnara, and A. Pegoretti, *J. Polym. Res*., **24**, 96 (2017).
63. A. Dorigato, M. Brugnara, G. Giacomelli, L. Fambri, and A. Pegoretti, *J. Ind. Textiles*, **45**, 1504 (2016).
64. W.S.J. Hummers and R.E. Offeman, *J. Am. Chem. Soc*., **80**, 1339 (1958).
65. N.I. Kovtyukhova, P.J. Ollivier, B.R. Martin, T.E. Mallouk, S.A. Chizhik, E.V. Buzaneva, and A.D. Gorchinskiy, *Chem. Mater*., **11**, 771 (1999).
66. R.H. Mehta. "Physical Constants of Various Polyamides," in *Polymers Handbook*, 4th ed., J. Brandrup, E.H. Immergut, and E.A. Grulke, Eds., Wiley-Interscience, New York, V/126 (1999).
67. A. Dorigato, A. Biani, W. Bonani, and A. Pegoretti, *J. Cellular Plast*., (in press).
68. G. Gedler, M. Antunes, V. Realinho, and J. Velasco, *Polym. Degrad. Stabil*., **97**, 1297 (2012).
69. A. Dorigato, M. Brugnara, and A. Pegoretti, *Adv. Polym. Technol*., (in press).
70. M. D'Amato, A. Dorigato, L. Fambri, and A. Pegoretti, *Express Polym. Lett*., **6**, 954 (2012).
71. M. Tokihisa, K. Yakemoto, T. Sakai, L.A. Utracki, M. Sepehr, J. Li, and Y. Simard, *Polym. Eng. Sci*., **46**, 1040 (2006).
72. X. Zhang, X. Tian, J. Zheng, X. Yao, W. Liu, P. Cui, and Y. Li, *J. Macromol. Sci., Part B: Phys*., **47**, 368 (2008).